

Characterization of the expression of the pro-metastatic Mena^{INV} isoform during breast tumor progression

Madeleine J. Oudin¹ · Shannon K. Hughes^{1,2} · Nazanin Rohani¹ ·
Mira N. Moufarrej² · Joan G. Jones⁵ · John S. Condeelis³ ·
Douglas A. Lauffenburger^{1,2} · Frank B. Gertler^{1,4}

Received: 24 August 2015 / Accepted: 7 December 2015 / Published online: 17 December 2015
© Springer Science+Business Media Dordrecht 2015

Abstract Several functionally distinct isoforms of the actin regulatory Mena are produced by alternative splicing during tumor progression. Forced expression of the Mena^{INV} isoform drives invasion, intravasation and metastasis. However, the abundance and distribution of endogenously expressed Mena^{INV} within primary tumors during progression remain unknown, as most studies to date have only assessed relative mRNA levels from dissociated tumor samples. We have developed a Mena^{INV} isoform-specific monoclonal antibody and used it to examine Mena^{INV} expression patterns in mouse mammary and human breast tumors. Mena^{INV} expression increases during tumor progression and to examine the relationship between Mena^{INV} expression and markers for epithelial or mesenchymal status, stemness, stromal cell types and hypoxic regions. Further,

while Mena^{INV} robustly expressed in vascularized areas of the tumor, it is not confined to cells adjacent to blood vessels. Altogether, these data demonstrate the specificity and utility of the anti-Mena^{INV}-isoform specific antibody, and provide the first description of endogenous Mena^{INV} protein expression in mouse and human tumors.

Keywords Breast cancer · Mena · Hypoxia · Stemness · Microenvironment · Metastasis

Abbreviations

DCIS	Ductal carcinoma in situ
EGF	Epidermal growth factor
EMT	Epithelial to mesenchymal transition
FFPE	Formalin fixed paraffin embedded
GFP	Green fluorescent protein
IP	Immunoprecipitation
LN	Lymph node
SMA	Smooth muscle actin
TMEM	Tumor microenvironment of metastasis

Madeleine J. Oudin and Shannon K. Hughes have contributed equally to this work.

Electronic supplementary material The online version of this article (doi:10.1007/s10585-015-9775-5) contains supplementary material, which is available to authorized users.

✉ Madeleine J. Oudin
mjoudin@mit.edu

- ¹ Koch Institute for Integrative Cancer Research, MIT, 76-317, 77 Massachusetts Ave, Cambridge, MA 02139, USA
- ² Department of Biological Engineering, MIT, Cambridge, MA 02139, USA
- ³ Department of Anatomy and Structural Biology, Albert Einstein College of Medicine, Bronx, NY 10461, USA
- ⁴ Department of Biology, MIT, Cambridge, MA 02139, USA
- ⁵ Integrated Imaging Program, Albert Einstein College of Medicine, Bronx, NY 10461, USA

Introduction

While metastasis remains the leading cause of death in cancer patients, the molecular mechanisms driving this process are incompletely understood. Changes within the primary tumor itself or in the microenvironment can lead to local invasion and ultimately metastasis. For example, during the epithelial to mesenchymal transition (EMT), cells can undergo changes in gene expression which endow carcinoma cells with aggressive, metastatic characteristics [1]. Increased matrix stiffening, collagen crosslinking and

integrin-dependent focal adhesion are also associated with breast tumorigenesis and can promote progression to an invasive and metastatic phenotype [2, 3]. Hypoxia, via stabilization of hypoxia-inducible factor (HIF1 α), regulates the expression of multiple genes that can lead to changes in anaerobic metabolism, angiogenesis, invasion and survival [4]. Finally, the tumor stroma plays an important role in promoting metastasis as recruitment of macrophages or bone marrow derived cells to the primary tumor site can increase cell migration, invasion and intravasation [5].

Mena, a member of the Ena/VASP family, is a known regulator of actin polymerization and cell:matrix, and cell:adhesion that is upregulated in various human epithelial tumors, including breast, pancreas, lung, colon and cervix [6]. In the MMTV–PyMT genetic model of breast cancer, genetic ablation of Mena significantly reduces in vivo tumor cell motility, intravasation and metastasis without altering mammary tumor burden, growth or histologic progression to carcinoma [7]. Mena-expressing cells are components of tumor microenvironment of metastasis (TMEM), tripartite structures comprised of a Mena-expressing tumor cell, an endothelial cell and a macrophage all contacting each other. TMEMs are sites of intravasation in mouse mammary tumors [8], and TMEM density correlates with risk of distant metastasis in ER–/HER2+ breast cancer patients [9, 10].

During tumor progression, Mena is alternatively spliced to produce multiple isoforms that can affect tumor cell phenotypes in different ways [6]. Expression of Mena11a, an isoform of Mena that contains an additional 21 amino acids in the EVH2 domain of Mena, is highly expressed in primary tumor cells, but downregulated in invasive cells [11], and has been shown to decrease motility in vivo and dampen invasion responses to EGF [12]. In two patient cohorts, quantitative immunofluorescence of a biomarker Mena^{calc} derived from the difference in expression levels of all Mena isoforms (“panMena”) and Mena11a showed that high Mena^{calc} levels are associated with poor disease-specific survival [13, 14].

Conversely, inclusion of the 19-amino acid sequence encoded by the ‘INV’ exon (Fig. 1a) in Mena promotes invasion, intravasation and metastasis by sensitizing cells to EGF, subsequently allowing them to invade in response to low concentrations of growth factor [12, 15]. Notably, the lack of a sensitive isoform-specific antibody capable of detecting Mena^{INV} in tumors has necessitated use of RT-PCR analysis of mRNA isolated from dissociated tumor tissues as a proxy for the protein. Using xenograft and spontaneous breast tumor models, we found that expression of Mena^{INV} mRNA is comparatively high in invasive cells collected by EGF chemotaxis from the primary tumor [11]. Furthermore, in cells isolated from fine needle aspirates (FNA) of breast human tumors, Mena^{INV} mRNA levels

were relatively higher in the subset of tumor cells that had traversed a human endothelial cell monolayer in in vitro intravasation assays [16]. Finally, in human breast cancer patients, relative levels Mena^{INV} mRNA in FNA biopsies from freshly resected breast tumor samples were observed to correlate with the number of TMEM sites found histological sections from the matched tumor tissue [16, 17]. However, the abundance and distribution of Mena^{INV} protein within primary tumors have not yet been determined. Given the relatively high expression of Mena^{INV} in invasive tumor cell subpopulations, and the ability of Mena^{INV} expression to enhance microenvironment-dependent metastatic phenotypes, reagents that allow for analysis of Mena^{INV} protein levels and distribution within histological sections of patient tumors might be used to gain insight into the biology of tumor progression and, potentially, as a prognostic biomarker.

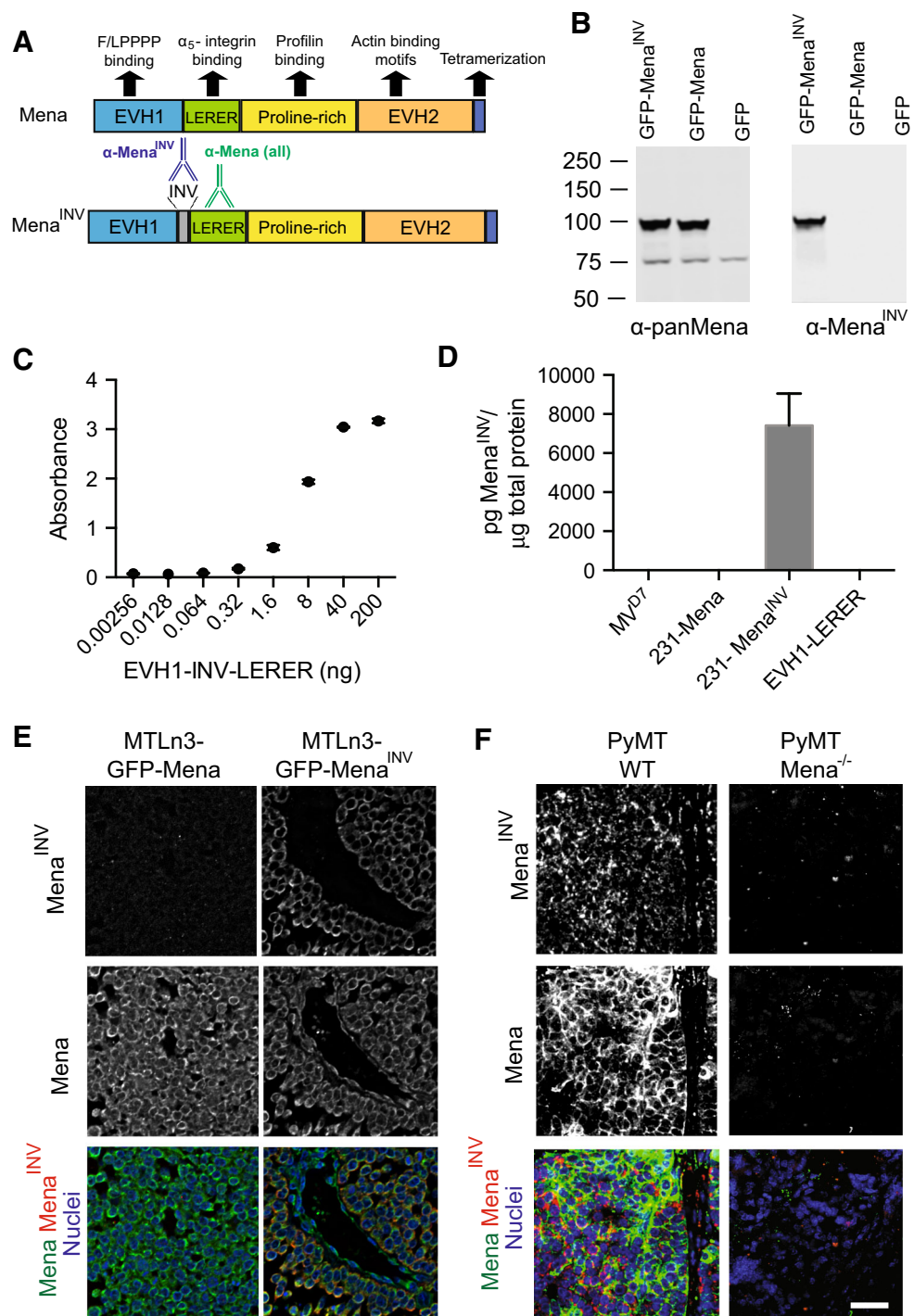
Using a newly generated isoform-specific antibody validated in three assays, we show that Mena^{INV} protein expression increases during tumorigenesis and progression and is correlated with blood vessel density. Furthermore, we show that while Mena^{INV} expression is inversely correlated with E-cadherin, it is not restricted to mesenchymal-like cells, is not detected in stromal cells, and does not correlate with increased proliferation, stemness, macrophage density, or hypoxia. These results provide insight into the spatiotemporal distribution of Mena^{INV} within primary tumors, key information needed to develop models to describe its pro-metastatic effects, and provide the basis for evaluating Mena^{INV} as potential biomarker for clinical use.

Results

Validation of the Mena^{INV} antibody for use in western blot, ELISA and immunohistochemistry

To analyze Mena^{INV} protein expression and distribution, we developed an isoform-specific monoclonal antibody that selectively recognizes the 19aa sequence (identical in human and mouse) encoded by the INV exon (“anti-INV”) [18] (Fig. 1a). Anti-INV recognized GFP-Mena^{INV}—but not GFP-Mena or GFP alone—in western blots of lysates of MDA-MB231 cells that express the corresponding constructs. Anti-panMena, which recognizes all known Mena isoforms [19], detected ectopic GFP-Mena, GFP-Mena^{INV} and endogenous Mena (Fig. 1b). We developed an ELISA assay to detect and to quantify Mena^{INV} levels in protein lysates. We confirmed the specificity of the ELISA assay using two peptides expressing either EVH1-LERER or EVH1-INV-LERER. Increasing the concentration of the EVH1-INV-LERER peptide correlated with an increase in

Fig. 1 Validation of the Mena^{INV} antibody. **a** Schematic diagram of cancer-relevant alternatively spliced Mena isoforms and in-house antibodies utilized for detection. **b** Western blot of MDA-MB231 cells overexpressing GFP, GFP-Mena or GFP-Mena^{INV}. Mena^{INV} antibody only recognizes GFP-Mena^{INV}, while the Mena antibody recognizes both isoforms. **c** Standard curve for Mena^{INV} ELISA assay, plotting concentration of pure recombinant protein EVH1-INV-LERER versus absorbance. Protein concentrations were estimated by comparison to purified recombinant Mena^{INV} mini-protein. **d** Mena^{INV} protein concentration in MV^{D7} fibroblasts, 231-Mena and 231-Mena^{INV} cultured cells, and using EVH1-LERER as a negative control, quantified by sandwich ELISA using anti-panMena for capture and anti-Mena^{INV} for detection. **e** Representative images of FFPE sections from Mtn3 tumors expressing GFP-Mena or GFP-Mena^{INV}, stained with Mena (green), Mena^{INV} (red) and DAPI (blue). Similarly, Mena^{INV} antibody only recognizes GFP-Mena^{INV}, while the Mena antibody recognizes both isoforms. **f** Staining for Mena and Mena^{INV} on an FFPE section from a wild-type PyMT mouse or a PyMT mouse null for Mena. Scale bar is 30 μm. (Color figure online)



signal as detected by the ELISA assay, while no signal was detected with the EVH1-LERER peptide (Fig. 1c). We then measured Mena^{INV} expression in lysates collected from MV^{D7} fibroblasts, which lack all three Ena/VASP proteins [20], MDA-MB-231 cells expressing ectopic GFP-Mena (“231-Mena”) or GFP-Mena^{INV} (“231-Mena^{INV}”). Using the ELISA assay, no signal above the assay detection limit for Mena^{INV} was detected in MV^{D7} fibroblasts, or

231-Mena cells; while a strong signal was detected in 231-Mena^{INV} cells (Fig. 1d). Together, these data confirmed the specificity of the antibody and quantitative nature of the ELISA assay.

Given that we have shown that at the mRNA level, Mena^{INV} expression is enriched in invasive cell populations of xenograft tumors, PyMT tumors [21], and in FNA biopsies of human breast tumors [16], we were interested in

visualizing the distribution of Mena^{INV} protein within tumors. The Mena^{INV} antibody was validated for use and specificity in staining of formalin-fixed paraffin embedded (FFPE) tumor sections by comparing anti-INV signals in xenografts of cells expressing GFP-Mena^{INV} or GFP-Mena (Fig. 1e). As expected, strong signal for Mena^{INV} was observed in GFP-Mena^{INV} xenograft tissue sections, but absent in GFP-Mena tumor sections. Secondly, we examined mammary carcinomas arising from transgenic MMTV–PyMT expression and found that Mena^{INV} was heterogeneously distributed in this model. Furthermore, as expected we did not detect specific Mena^{INV} signal in tissue sections of tumors isolated from Mena knockout mice carrying the MMTV–PyMT transgene, used here as a negative control (Fig. 1f). These data confirm the specificity and utility of the antibody for use in immunodetection of Mena^{INV} in FFPE tissue sections.

Mena^{INV} expression in tumors is heterogeneous, but increases during progression in mouse and human samples

Next, we examined Mena and Mena^{INV} staining in normal mammary gland fat pad tissue and in advanced MMTV–PyMT tumors by immunofluorescence of FFPE sections (Fig. 2a, b). While Mena is widely expressed in ducts, we found low, heterogeneous staining for Mena^{INV} in normal ductal structures within the mammary gland, with significantly stronger Mena^{INV} staining intensity in tumor tissue (Fig. 2c). We then asked if Mena^{INV} is expressed in cells within non-invasive tumor structures with intact basement membranes, marked by staining with Laminin, and found that Mena^{INV} detectable in encapsulated pre-invasive tumor structures.

We then studied the relationship between Mena and Mena^{INV} expression during tumor progression in the MMTV–PyMT model [22]. Overall, we observed heterogeneous Mena^{INV} staining in subsets of Mena-expressing cells in MMTV–PyMT tumors (Fig. 2e). Specifically, there were significant increases in both Mena and Mena^{INV} staining in both adenoma and carcinoma tumor regions relative to hyperplasia (Fig. 2f, g). Together, these data suggest that in the MMTV–PyMT model Mena and Mena^{INV} expression increases during progression from hyperplasia to adenoma, with no further increases during progression to carcinoma.

Next, we examined Mena and Mena^{INV} protein expression and localization in a small cohort of both metastatic and non-metastatic human breast tumors (tumor characteristics described in Fig S1). We found that while Mena is expressed at high levels in ductal structures in non-metastatic tumors (Fig. 3a–c) only low levels of Mena^{INV}

were detected. As shown in the PyMT mouse model, we found robust levels of Mena^{INV} in structures characterized as ductal carcinoma in situ (DCIS), which are known to contain an intact basement membrane (Fig. 3d–f), with both isoforms expressed in these tissues. Finally, relatively higher levels of Mena^{INV} were observed in metastatic patients. Patients with metastatic disease showed increased percentage of cells expressing Mena^{INV} (Fig. 3j), as well as increased levels of Mena^{INV}, as detected by quantitative immunofluorescence (Fig. 3l). Levels of Mena were not significantly different between non-metastatic and metastatic cases (Fig. 3k). Overall, these data demonstrate that Mena^{INV} expression increases during tumor progression in both mouse and human tumors.

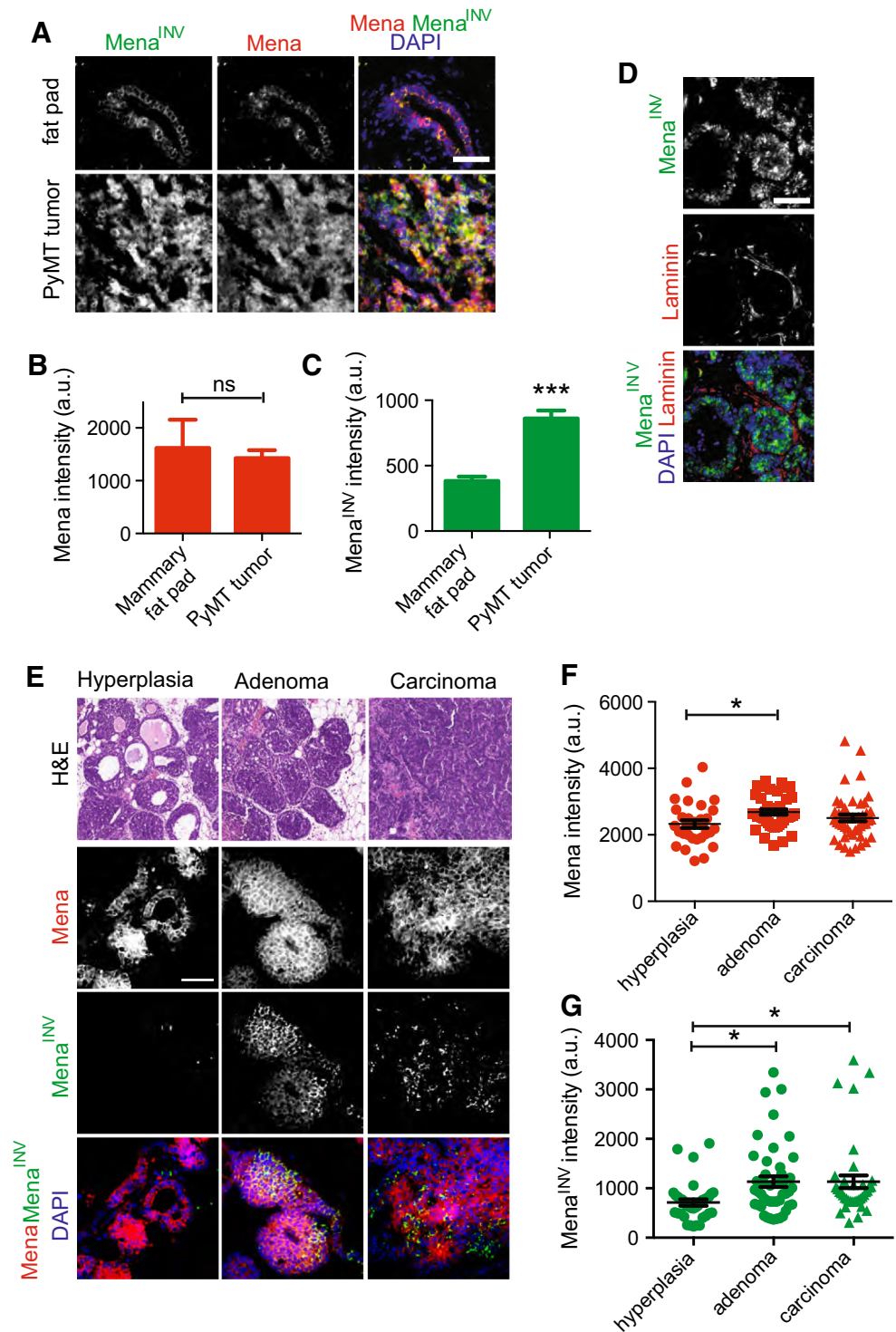
Mena^{INV} is not expressed in macrophages, endothelial cells or fibroblasts

The tumor microenvironment is composed of a variety of tumor and stromal cells, which can also contribute to tumor progression [5]. We were interested in investigating whether Mena^{INV} was expressed in endothelial cells, macrophages and fibroblasts within tumors. We used established markers to stain for all three subpopulations in PyMT tumors: Iba1 for macrophages (Fig. 4a); α SMA (smooth muscle actin) for fibroblasts (Fig. 4b); CD31 for endothelial cells (Fig. 4c). We did not detect Mena^{INV} signal in any of the cells expressing these markers and conclude that Mena^{INV} is either absent or expressed at low levels in these stromal subtypes.

Mena^{INV} expression is not restricted to cells that have undergone EMT

To characterize the identity of the cells that express Mena^{INV} in the tumor compartment, we compared the distribution of anti-INV staining to markers of tumor cell phenotype. First, we wondered if expression of Mena^{INV} was associated with EMT, a process that has been associated with increased metastatic potential [23]. Antibodies to E-Cadherin and vimentin, markers for epithelial and mesenchymal phenotypes respectively, were used to examine levels of Mena^{INV} varied throughout mouse and human tumors in relation to EMT. Line scans of the signal intensities showed regions that appeared to have relatively high Mena^{INV} and low E-cadherin signals (Fig. 5a). Quantitative analysis throughout entire image fields revealed a significant, inverse correlation between relative levels of Mena^{INV} and of E-cadherin (Fig. 5b, c): Mena^{INV} was detected in 62 and 74 % of vimentin positive cells in human and mouse tumors, respectively (Fig. 5d), however,

Fig. 2 Mena^{INV} expression increases during tumor progression. **a** Representative images of FFPE sections from a normal mammary fat pad tissue from an adult mouse and an advanced MMTV–PYMT tumor stained for Mena, Mena^{INV} and DAPI. *Scale bar* is 30 μ m. Quantification of Mena (**b**) and Mena^{INV} (**c**) staining intensity in mammary fat pad versus advanced tumor. **d** Representative images of FFPE sections from an MMTV–PYMT tumor stained for Mena^{INV}, the basement member laminin and DAPI. *Scale bar* is 30 μ m. **e** Representative images of areas from MMTV–PYMT tumor sections depicting hyperplasia, adenoma and carcinoma tumor. H&E image depicts histology of area chosen for for Mena, Mena^{INV} and DAPI staining. *Scale bar* is 100 μ m for H&E image, and 30 μ m for fluorescent images. Quantification of Mena (**f**) and Mena^{INV} (**g**) staining intensity in different areas of PyMT tumors. Data pooled from four tumors, with at least four fields of view per sample. *Each dot* represents a field of view. *Asterisk* indicates significant difference by *t* test (**p* < 0.05)



vimentin was detected in only 27 and 18 % of Mena^{INV} - positive cells in human and mouse tumors, respectively. Together, these results indicate that while Mena^{INV} protein distribution is inversely correlated with E-Cadherin, it is observed frequently in cells lacking vimentin, a canonical marker for passage through EMT.

Mena^{INV} expression is not enriched with cells expressing proliferation and stem cell markers

More recently, EMT has been associated with the gain of stem cell characteristics, which endow cells with the ability to metastasize and colonize more efficiently [24]. We

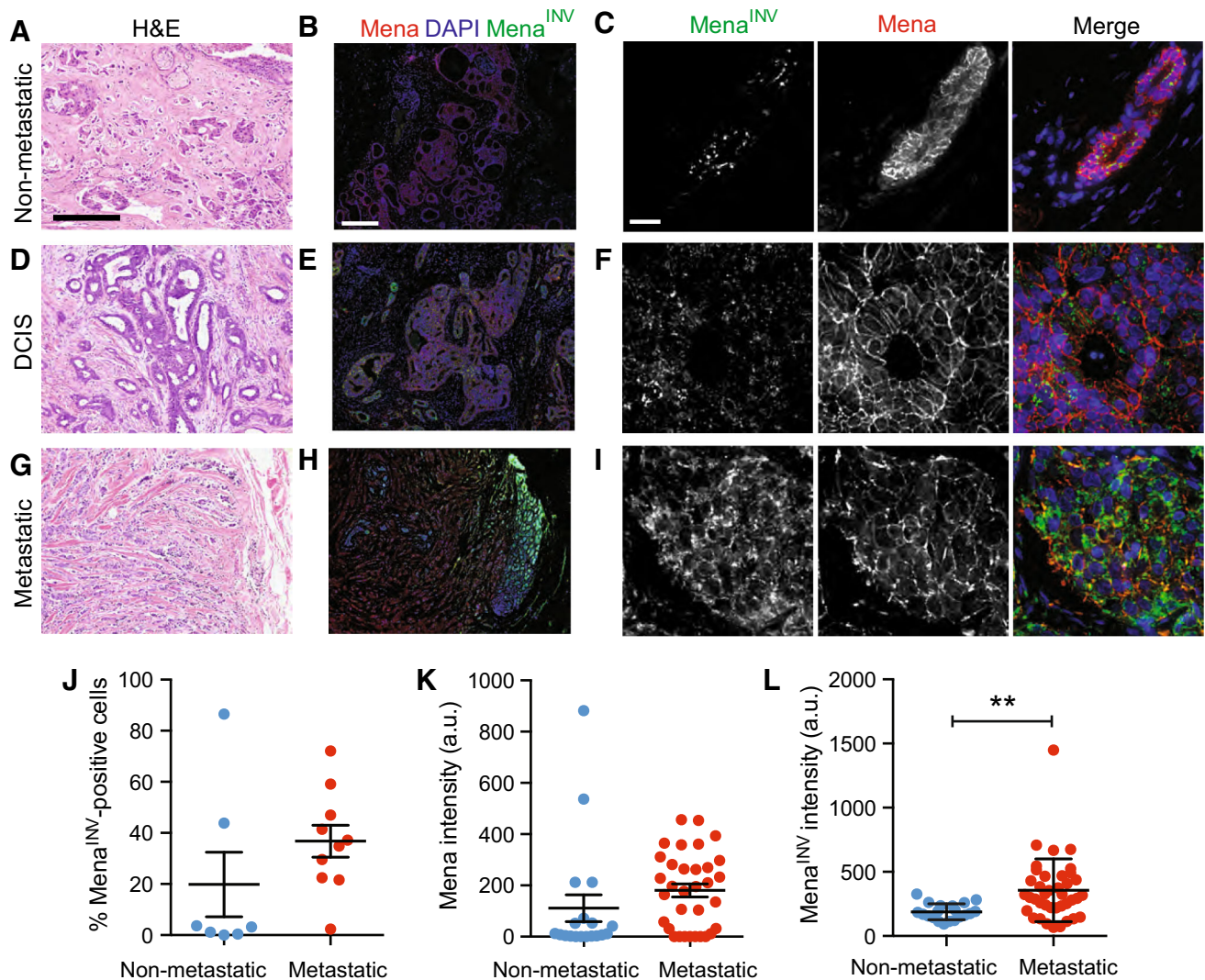


Fig. 3 Mena^{INV} expression patterns in human breast cancer. Representative images of human breast tumor FFPE sections with H&E staining (**a, d, g**), low (**b, e, h**) and high (**c, f, i**) magnification images of immunofluorescence staining for Mena (red) and Mena^{INV} (green). Images are from a non-metastatic (**a–c**), DCIS (**d–f**) and metastatic tumor (**g–i**). Scale bar for **a, d, g** is 300 μ m, for **b, e, h** is 100 and 30 μ m for **c, f, i**. **j** Quantification of the percentage of total

cells (as counted by DAPI staining) expressing Mena^{INV} within a 40X field. Quantification of Mena (**k**) and Mena^{INV} (**l**) staining intensity in non-metastatic and metastatic human tumor samples. Data pooled for three metastatic and three non-metastatic samples, with at least three fields of view per sample. Each dot represents a field of view. Asterisk indicates significant difference by *t* test (***p* < 0.01). (Color figure online)

investigated whether expression of Mena^{INV} was associated with the proliferation or acquisition of stem cell characteristics. First, we examined the proliferation levels of Mena^{INV}-positive cells, by staining for the proliferation marker Ki67 (Fig. 6a). In both mouse and human tumors, approximately 30 % of Mena^{INV} cells were Ki67-positive. Conversely, approximately 50 % of Ki67-positive cells were Mena^{INV}-positive (Fig. 6b, c). These data suggest that Mena^{INV} expression is not restricted to highly proliferative cells. Secondly, we examined Mena^{INV} expression relative to two known stem cell markers in mouse PyMT tumors, ALDH and CD133, whose expression has been associated

with stemness (Fig. 6d). Indeed, recent studies have shown that cells expressing high levels of CD133 showed higher invasive potential and drug resistance, while cells that were ALDH- and CD133-positive were highly tumorigenic [25–27]. As expected, we observed a positive correlation between CD133 and ALDH expression (Fig. 6e); however, no significant association between cells expressing Mena^{INV} and those expressing canonical stem cell markers. Only 15 and 23 % of Mena^{INV}-positive cells expressed CD133 or ALDH, respectively (Fig. 6f, h). Similarly, approximately 28 and 41 % of CD133- and ALDH-positive cells, respectively, expressed Mena^{INV} in PyMT tumors

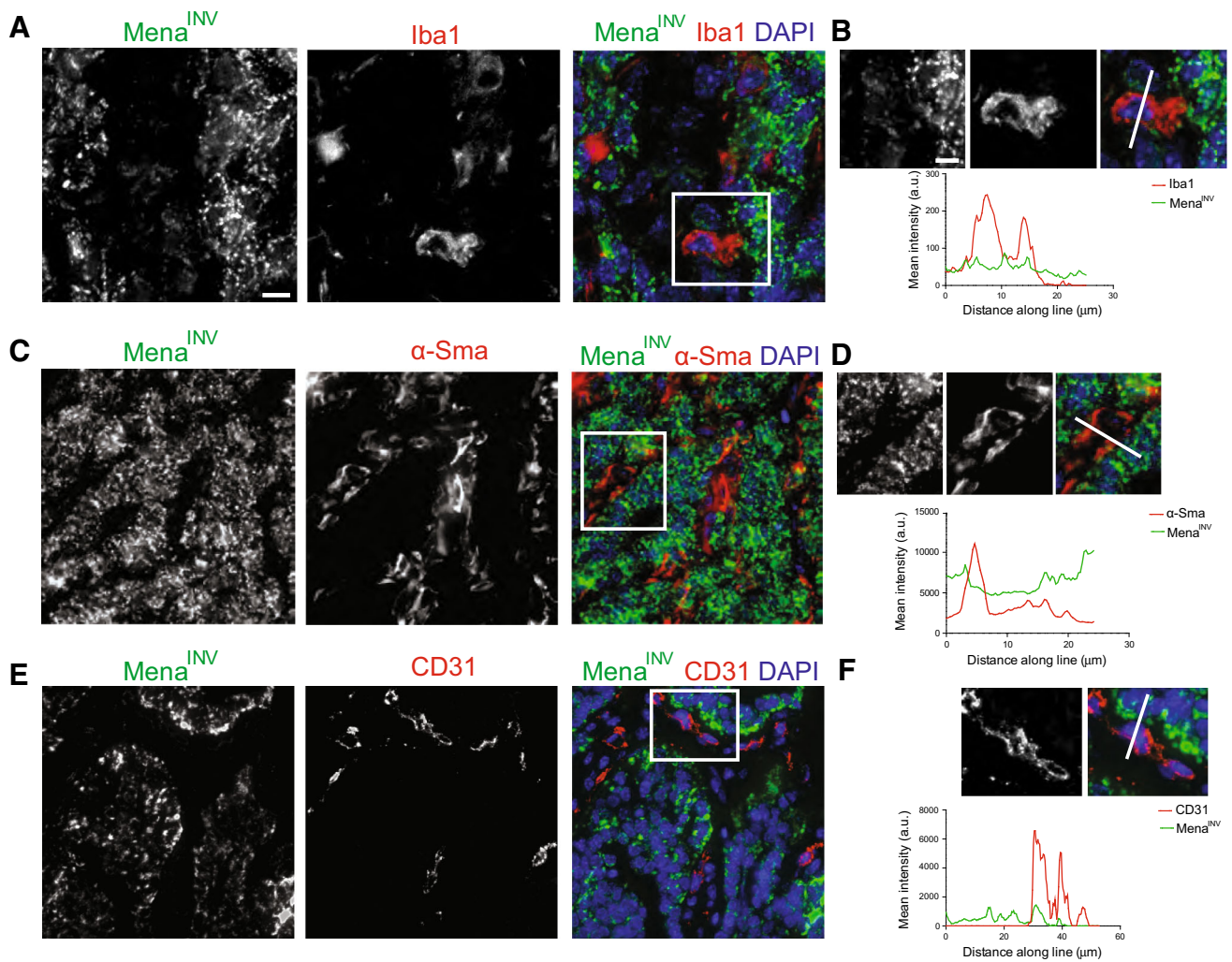


Fig. 4 Mena^{INV} expression is restricted to the tumor compartment. Representative images of staining for Mena^{INV} and the macrophage marker Iba1 (a, b), the fibroblast marker αSMA (c, d) and the

endothelial cell marker CD31 (e, f). **b–d** Magnification of boxed area and signal intensity for both markers is quantified along the white line. Scale bar for a, c, e is 30 and 10 μm for b, d, f

(Fig. 6f, h). These data indicate that Mena^{INV} is expressed in both stem and non-stem cell populations within advanced tumors. We compared Mena^{INV} and CD133 or ALDH staining intensity in different regions of PyMT tumors and observed no significant correlation between Mena^{INV} signal and the levels of these stem cell markers.

Mena^{INV} expression is high in vascularized tumor areas

Dissemination of primary tumor cells occurs primarily through the vasculature and lymphatics. We examined patterns of Mena^{INV} expression relative to blood vessels in mouse and human tumors. In both mouse and human

tumors, we found that Mena^{INV} expression was not restricted to cells adjacent to blood vessels (Fig. 7a, b). However, there was a significant correlation between Mena^{INV} expression levels and blood vessel density in both non-metastatic and metastatic human tumors (Fig. 7c). Together, these data confirm that while Mena^{INV} expression is associated with higher blood vessel density, it is not restricted to expression in cells adjacent to the vasculature.

Blood vessel density can also affect oxygen levels within a tumor, which in turn, can drive metastatic phenotypes. Using hypoxyprobe to label hypoxic tumor areas [28], we quantified Mena^{INV} staining intensity in PyMT–MMTV tumors relative to hypoxia (Fig. 7d, e) and determined that Mena^{INV} expression was not restricted to hypoxic areas within the tumor.

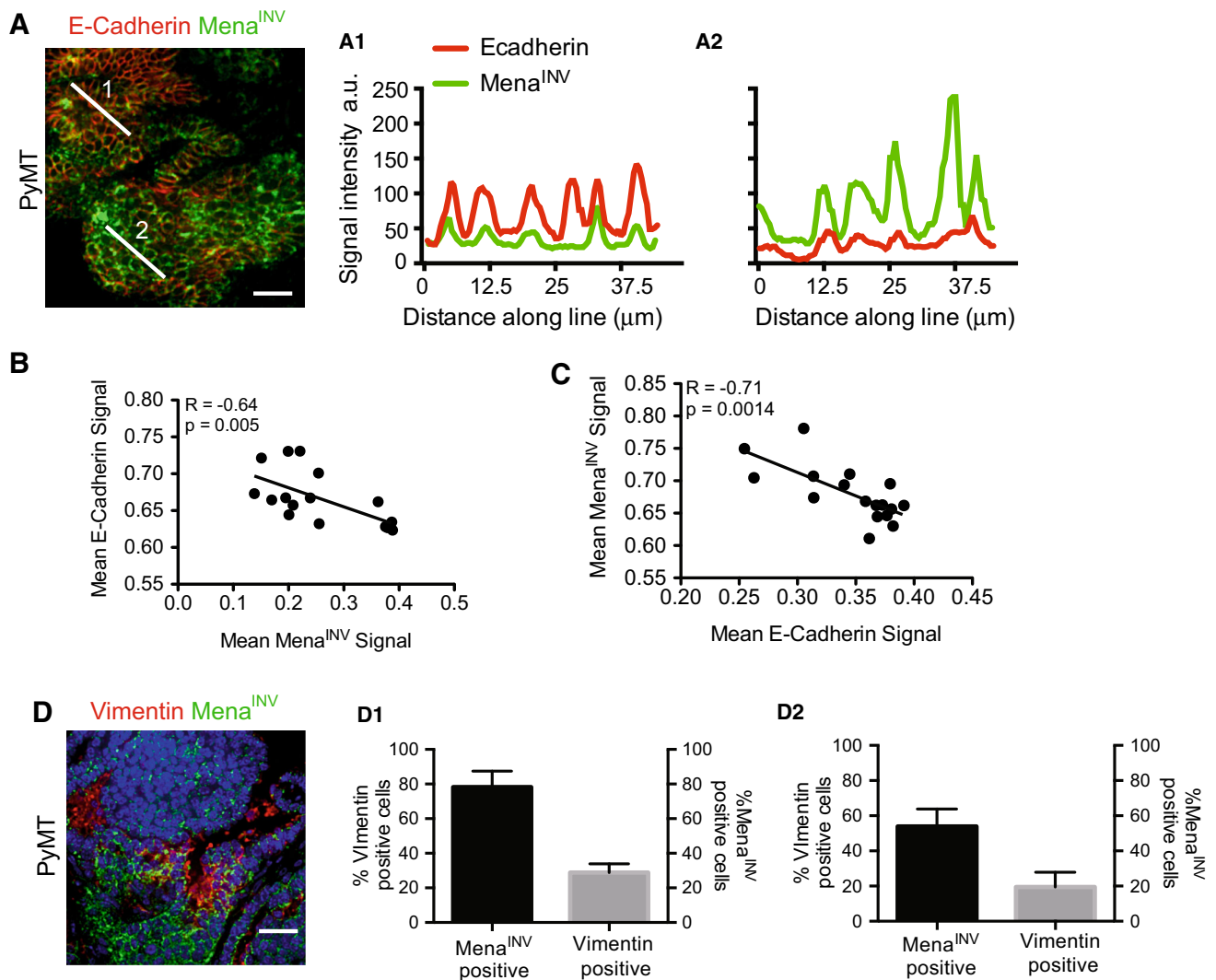


Fig. 5 Mena^{INV} expression and EMT markers. **a** MMV-PyMT tissue section stained for Mena^{INV} (green) and the epithelial marker ECadherin (green). **a1-2** Intensity of Mena^{INV} and ECadherin signal along two lines shown in **a**. **b** Mean fluorescence signal intensity plotted for Mena^{INV} intensity >0.55 and E-Cadherin intensity <0.5. **c** Mean fluorescence signal intensity plotted for E-Cadherin intensity >0.55 and Mena^{INV} intensity <0.5. Raw pixel values were normalized by the range of intensities in each image. $n = 5$ mice, three image fields per tumor. **d** MMTV-PyMT tissue section stained for Mena^{INV} (red) and vimentin (green). **d1** Black bar quantifies the

fraction of vimentin-positive cells that are also Mena^{INV}-positive, grey bar quantifies the fraction of Mena^{INV}-positive cells that are also vimentin-positive. Results are shown as mean \pm SEM = 2 mice, 5–7 image fields per tumor for **f**, **g**. Scale bar = 20 μ m for **f**, **g**. **d2** Black bar quantifies the fraction of vimentin+ cells that are also Mena^{INV}+ in human sections, grey bar quantifies the fraction of Mena^{INV}-positive cells that are also vimentin+. Results are shown as mean \pm SEM, $n = 2$, 5–7 image fields per tumor for **f**, **g**. (Color figure online)

Discussion

The data presented here provide the first characterization of endogenous Mena^{INV} protein expression in mouse breast cancer models and in human invasive ductal carcinomas. Our studies reveal that expression of Mena^{INV} is heterogeneously distributed in tumors and that Mena^{INV} expression can be detected in early tumors with increasing levels during early tumor progression. Our comparison of Mena^{INV} staining to the distributions of well-established

markers provides insight into the nature of the tumor cells that express Mena^{INV}.

We developed a Mena^{INV} isoform-specific monoclonal antibody, and demonstrated its specificity and functionality in ELISA and Western blot assays, and for immunodetection of endogenously expressed protein in human and mouse sections of FFPE tumor tissue. Our analysis provides important information on the properties of cells that express Mena^{INV}, allowing us to gain further insight into the potential mechanisms by which it drives metastasis. We

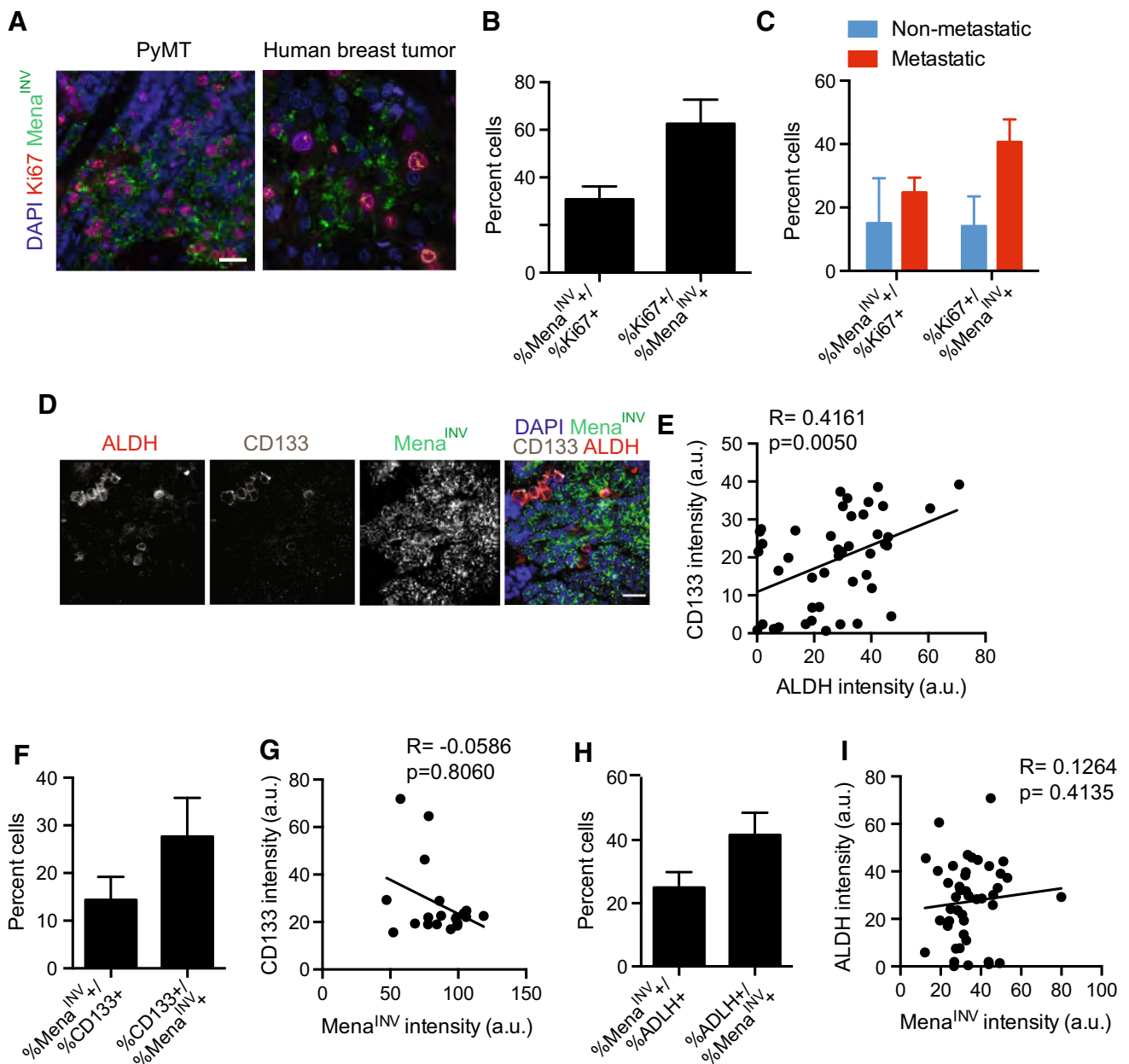


Fig. 6 Mena^{INV} expression is not restricted to cancer stem cells. **a** Representative images of PyMT tumors and human breast tumors stained for Mena^{INV} (green) and Ki67 (red). Scale bar is 30 μm. **b** Quantification of the fraction of Mena^{INV}-positive cells that are also Ki67-positive and the fraction of Ki67-positive cells that are also Mena^{INV}-positive in mouse PyMT tumors. Results are shown as mean ± SEM, n = 2 mice, five image fields per mouse. **c** Quantification of the fraction of Mena^{INV}-positive cells that are also Ki67-positive and the fraction of Ki67-positive cells that are also Mena^{INV}-positive in human breast tumors from metastatic and non-metastatic patients. Results are shown as mean ± SEM, n = 3 tumors, five image fields per tumor. **d** Representative images of PyMT tumors

stained for Mena^{INV} (green) and the stem cell markers ALDH (red) and CD133 (blue). **e** Positive correlation between staining intensity for CD133 and ALDH in PyMT sections. **e** Quantification of the fraction of Mena^{INV}-positive cells that are also CD133-positive and the fraction of CD133-positive cells that are also Mena^{INV}-positive in mouse PyMT tumors. **f** Correlation between Mena^{INV} and CD133 staining intensity in PyMT tumors. **g** Quantification of the fraction of Mena^{INV}-positive cells that are also ALDH-positive and the fraction of ALDH-positive cells that are also Mena^{INV}-positive in mouse PyMT tumors. **f** Correlation between Mena^{INV} and ALDH staining intensity in PyMT tumors. Results are shown as mean ± SEM, n = 4 tumors, 3–5 image fields per sample. (Color figure online)

show that Mena^{INV} expression is not enriched in cells with increased proliferation as identified by Ki67, or stemness, as identified by cancer stem cell markers CD133 and

ALDH. Furthermore, we show that within the tumor microenvironment, Mena^{INV} expression is absent from macrophages, endothelial cells and fibroblasts, suggesting

Fig. 7 Mena^{INV} expression is high in vascularized areas.

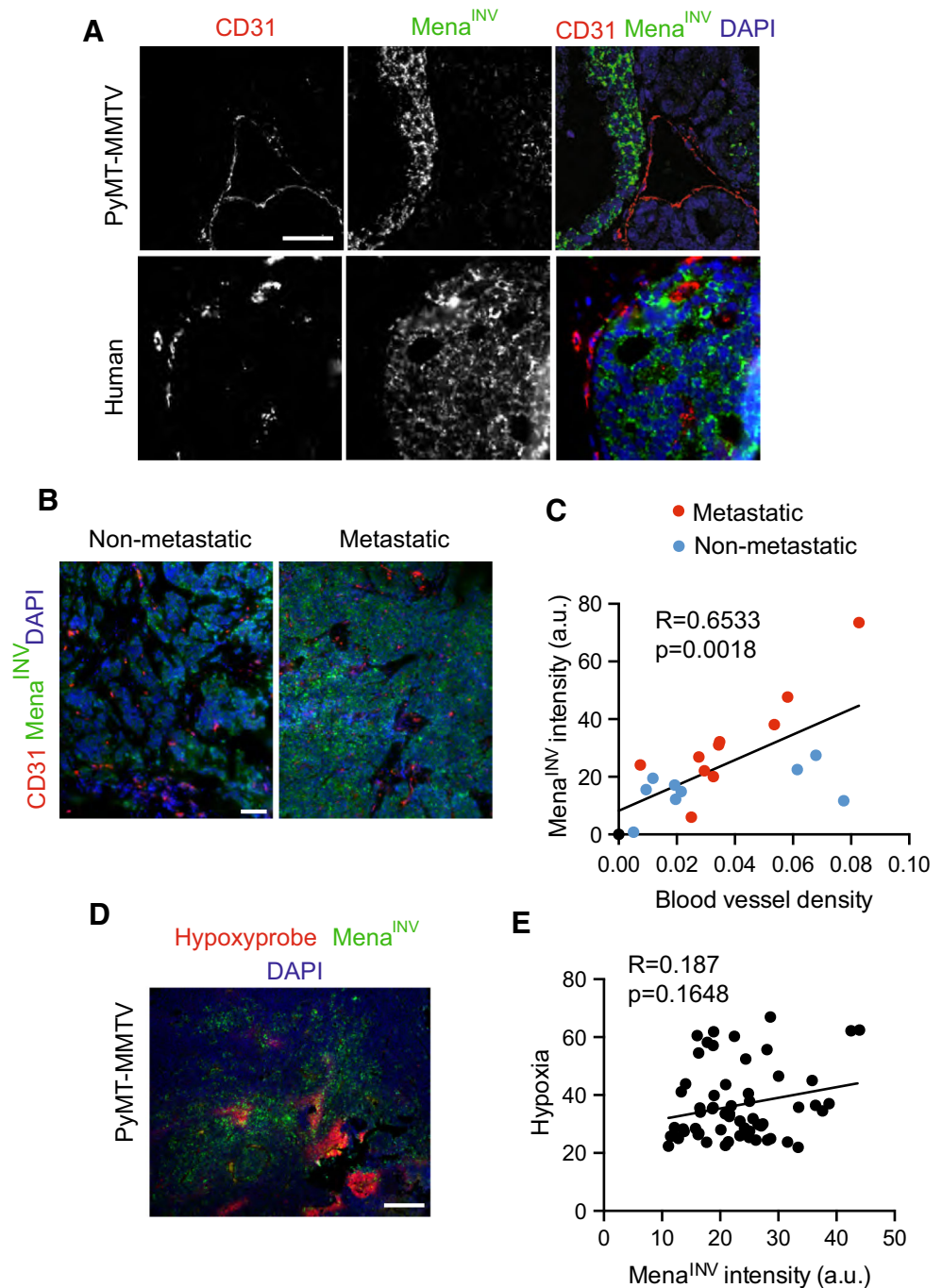
a MMTV–PyMT and human tissue section stained for Mena^{INV} (green) and the endothelial marker CD31 (red). Scale bar is 30 μ m.

b Representative images of human breast tumors from a metastatic and non-metastatic tumor, showing staining for Mena^{INV} (green) and the endothelial marker CD31 (red). Scale bar is 100 μ m.

c Correlation between blood vessel density and Mena^{INV} staining intensity in human breast tumors. Data pooled for three metastatic and three non-metastatic samples, with 2–3 fields of view per sample. Each dot represents a field of view.

e Representative image from an MMTV–PyMT tumor stained for Mena^{INV} and hypoxic areas, which were detected using the Hypoxyprobe. Scale bar is 100 μ m.

f Correlation between hypoxia (as measured by intensity of the Hypoxyprobe staining) and Mena^{INV} staining intensity in PyMT–MMTV tumors. Data pooled from 2 tumors, with over 40 fields of view analyzed. Each dot represents a field of view. (Color figure online)



it is likely restricted to the tumor compartment. Finally, we show that while expression of Mena^{INV} is high in areas of high blood vessel density, it is heterogeneous within the primary tumor and not confined to cells adjacent to blood vessels. In fact, Mena^{INV} expression can also be detected in non- (or perhaps pre-) invasive tumor compartments with an intact basement membrane, suggesting that Mena^{INV} is expressed early during breast cancer progression and in multiple locations. Together, these data suggest the role of

Mena^{INV} in promoting invasion and metastasis is not restricted to a role only in perivascular tumor cells at sites of intravasation, like those found in TMEM. This finding is consistent with our previous work showing that Mena^{INV} promotes matrix degradation, paracrine signaling with macrophages, discohesive tumor morphology and increased tumor cell motility [12, 15, 29]. As recent work demonstrates that the Mena-expressing tumor cell in TMEM is relatively stable [8], it will be interesting to

determine whether and how Mena^{INV} may contribute to TMEM assembly and function.

We have yet to identify what aspects of the tumor microenvironment drive Mena^{INV} expression or the identity of the splicing factor(s) responsible for INV inclusion. During tumor progression, EMT-associated transcription factors including Twist, Snail and Zeb1 drive a wide variety of alternative splicing that contribute to the mesenchymal phenotype and drive increased motility [30]. Here, we find that Mena^{INV} expression in mouse and human tumors is not restricted to either epithelial or mesenchymal cells, suggesting that a full passage through EMT is not required for INV inclusion. A variety of other microenvironmental characteristics can facilitate tumor progression and could be responsible for promoting inclusion of INV. We initially hypothesized that increases in blood vessel density or changes in oxygen availability might drive INV inclusion. However, we found that Mena^{INV} expression is not confined to hypoxic or highly vascularized areas within tumor, suggesting that these factors alone may not be sufficient to induce Mena^{INV} expression.

Changes in extracellular matrix composition or mechanical stimuli and secretion of a variety of soluble factors from tumor-associated stroma or the immune system also play an important role during tumor progression. We hypothesize that stiffness changes in combination with stromal factors will inclusion of the INV exon. Future work, using in part the assays described in this manuscript, will focus on how these combined stimuli might drive Mena^{INV} expression. Once the signals that trigger Mena^{INV} protein accumulation are defined, it will be interesting to determine whether expression of other cancer relevant protein isoforms is regulated coordinately with Mena^{INV}. Whether this substantial microenvironment-dependent increase in Mena^{INV} protein arises predominately from changes in INV exon inclusion in its mRNA or involves additional levels of regulation is also under investigation.

The development of the isoform specific antibody will also help advance the development of Mena isoform assessment as prognostic markers in cancer. Efforts are currently underway to determine whether analysis of Mena^{INV} protein levels, either alone or in combination with other prognostic metrics associated with Mena (e.g. Mena^{Calc} [13] or TMEM [9]), provides clinically useful information. More recently, an additional Mena isoform, Mena Δ V6, has been identified in some mesenchymal-like tumor cell lines [31]. It will be interesting to compare the distributions of all Mena protein isoforms throughout tumor progression. Finally, we have shown that Mena^{INV} expression sensitizes cells to several growth factors, whose signaling pathways are targets of clinical trials for

metastatic breast cancer [32]. Monitoring expression of Mena^{INV} in tumors might help optimise drug treatment for specific patients, as well as provide a means to monitor for acquired resistance to tyrosine kinase inhibitors.

Materials and methods

Antibodies

The following antibodies were used for immunohistochemistry: CD31 (R&D Systems, AF806), Vimentin (BD, RV202), Ecadherin (CST, 24E10), panMena [19], Ki67 (CST #9037), CD133 (EBioscience, clone 13A4), ALDH (BD, Clone 44), Iba1 (Abcam ab15690), α SMA (Sigma clone 1A4).

Production of anti-INV monoclonal antibody

Rabbit monoclonal antibodies were generated by Epitomics, INC. Animals were immunized with a peptide containing the sequence encoded by the INV exon. Clones were screened for Mena^{INV} specificity in Western blot assays and by immunostaining of FFPE tumor sections from wild type or Mena-null mice (Fig S1).

Anti-INV ELISA

Mena^{INV} protein levels in lysates were quantified by a custom sandwich ELISA. Anti-panMena antibody (1.8 μ g/mL) was coated overnight at 4 °C in 96-well Nunc Maxisorb plates (Sigma). After washing with PBS + 0.5 % Tween-20, assay plates were blocked at 25 °C with Licor Odyssey Blocking Buffer (Licor) and lysates were added overnight at 4 °C. Anti-Mena^{INV} antibody (0.38 μ g/mL) was added for 2 h at 25 °C. Anti-rabbit horseradish peroxidase secondary antibody (1:4000) (Millipore) and TMB substrate (Sigma) were used for detection. Recombinant proteins that contained a 6XHis-tagged Mena-EVH1-INV-LERER sequence or a control 6XHis-tagged Mena-EVH1-LERER construct that lacks the 19 residue INV peptide sequence were utilized to create a standard curve via four-parameter logistic regression in MATLAB, or act as a negative control, respectively. Relative protein concentrations were normalized to total protein content in μ g.

Cell culture

All breast cancer cell lines were obtained from ATCC and cultured in DMEM + 10 % FBS (Hyclone). Cell lines were engineered to stably express 10–15 fold higher levels of Mena isoforms more than wild-type cell lines.

Mouse models

All animal experiments were approved by the MIT Division of Comparative Medicine. PyMT–MMTV mice at 12 weeks of age were injected with 10 mg/kg Hypoxyprobe 1 h before sacrifice. To detect hypoxic areas, we used the Hypoxyprobe kit according to the manufacturer's protocol [28]. We injected 60 mg/kg of Piminidazole-HCl IP 1 h before sacrificing mice. Signal was then detected by immunostaining. Dissected tumors were dissociated using lysis buffer (see below) and mortar and pestle.

Western blotting

MDAMB231 expressing different Mena isoforms were lysed in 25 mM Tris, 150 mM NaCl, 10 % glycerol, 1 % NP 40 and 0.5 M EDTA with a protease Mini-complete protease inhibitors (Roche) and a phosphatase inhibitor cocktail (PhosSTOP, Roche) at 4 °C. Protein lysates were separated by SDS-PAGE, transferred to a nitrocellulose membrane, blocked with Odyssey Blocking Buffer (LiCor), incubated in primary antibody overnight at 4 °C. Proteins were detected using Licor secondary antibodies.

Immunostaining

Tumors from MMTV–PyMT mice were fixed in 10 % buffered formalin and embedded in paraffin. Sections from FFPE human breast cancer tumors were obtained from Dr. Joan Jones. Tissue sections (5 µm thick) were deparaffinized followed by antigen retrieval using Citra Plus solution (Biogenex). After treatment with 3 % H₂O₂, sections were blocked with serum and incubated with primary antibodies overnight at 4 °C. Fluorescently labeled secondary antibodies were added at 25 °C for 2 h. For detection of Mena^{INV} in FFPE sections, the INV antibody was biotinylated, followed by amplification with streptavidin-horseradish peroxidase, tyramide-biotin amplification (Perkin Elmer), and detection with a fluorescently tagged streptavidin antibody. Serial Z series image stacks were collected using a DeltaVision microscope controlled by Softworx software (GE Health) with a 40 × 1.3 NA plan-apo objective and deconvolved using Softworx. Images were then analyzed using ImageJ.

Image analysis

For Fig. 2, images within each panel were taken with the same settings and can be compared. However, panels a, d, e cannot be directly compared for intensity readings. Tumor area was delimited using DAPI staining, and intensity of signal was measured in each field of view using ImageJ. For Fig. 3, all images were acquired simultaneously and

intensity can be compared within the figure. For Figs. 3g, 5d, 6a–d, f, h, analysis of expression of markers was done on a per cell basis in multiple fields of view from multiple tissue samples. The number of positive cells for a specific marker was made relative to the total number of DAPI-positive cells in the field of view. For Fig. 5, custom written Matlab scripts were used for image analysis of ECadherin levels. For Fig. 7, blood vessel density was quantified using ImageJ, quantifying the area covered by blood vessels as marked by CD31 staining relative to the area of the field of view.

Acknowledgments This work was supported by Department of Defense Breast Cancer Research Program Grants W81XWH-10-1-0040 to SKH and W81XWH-13-1-0031 to MJO, NIH Grant U54-CA112967 to FBG and DAL and GM58801 to FBG, funds from the Ludwig Center at MIT to FBG and NR, the KI NCI Core Grant P30-CA14051, and CA150344 to JC and CA100324 for JJ, JJ, JC and FG are compensated members of the scientific advisory board of MetaStat. No funding was provided by MetaStat for this work. We thank the Histology facilities in the KI Swanson Biotechnology Center for support. We thank Evanthia Roussos for gifts of tumor tissue.

Author contributions MJO designed and performed experiments, data analysis and prepared the manuscript. SKH developed and validated the INV antibody, designed and performed experiments and completed data analysis. NR performed immunostaining experiments and image analysis. MNM developed Mena^{INV} ELISA, performed experiments and completed data analysis. FBG and DAL guided overall experimental design. JJ and JC contributed human tissue sections and interpretation of them. All authors commented on the manuscript.

References

- Hanahan D, Weinberg RA (2011) Hallmarks of cancer: the next generation. *Cell* 144(5):646–674
- Levental KR, Yu H, Kass L, Lakins JN, Egeblad M, Erler JT, Fong SFT, Csiszar K, Giaccia A, Wenginger W, Yamauchi M, Gasser DL, Weaver VM (2009) Matrix crosslinking forces tumor progression by enhancing integrin signaling. *Cell* 139(5):891–906
- Lu P, Weaver VM, Werb Z (2012) The extracellular matrix: a dynamic niche in cancer progression. *J Cell Biol* 196(4):395–406
- Pouyssegur J, Dayan F, Mazure NM (2006) Hypoxia signalling in cancer and approaches to enforce tumour regression. *Nature* 441(7092):437–443
- Joyce JA, Pollard JW (2009) Microenvironmental regulation of metastasis. *Nat Rev Cancer* 9(4):239–252
- Gertler F, Condeelis J (2011) Metastasis: tumor cells becoming MENAcing. *Trends Cell Biol* 21(2):81–90
- Roussos ET, Wang Y, Wyckoff JB, Sellers RS, Wang W, Li J, Pollard JW, Gertler FB, Condeelis JS (2010) Mena deficiency delays tumor progression and decreases metastasis in polyoma middle-T transgenic mouse mammary tumors. *Breast Cancer Res* 12(6):R101
- Harney AS, Arwert EN, Entenberg D, Wang Y, Guo P, Qian B-Z, Oktay MH, Pollard JW, Jones JG, Condeelis JS (2015) Real-time imaging reveals local, transient vascular permeability, and tumor

- cell intravasation stimulated by TIE2hi macrophage-derived VEGFA. *Cancer Discov*
9. Robinson BD, Sica GL, Liu Y-F, Rohan TE, Gertler FB, Condeelis JS, Jones JG (2009) Tumor microenvironment of metastasis in human breast carcinoma: a potential prognostic marker linked to hematogenous dissemination. *Clin Cancer Res* 15(7):2433–2441
 10. Rohan TE, Xue X, Lin H-M, D'Alfonso TM, Ginter PS, Oktay MH, Robinson BD, Ginsberg M, Gertler FB, Glass AG, Sparano JA, Condeelis JS, Jones JG (2014) Tumor microenvironment of metastasis and risk of distant metastasis of breast cancer. *J Natl Cancer Inst* 106(8):1–11
 11. Goswami S, Philippar U, Sun D, Patsialou A, Avraham J, Wang W, Di Modugno F, Nistico P, Gertler FB, Condeelis JS (2009) Identification of invasion specific splice variants of the cytoskeletal protein Mena present in mammary tumor cells during invasion in vivo. *Clin Exp Metastasis* 26(2):153–159
 12. Roussos ET, Balsamo M, Alford SK, Wyckoff JB, Gligorijevic B, Wang Y, Pozzuto M, Stobezki R, Goswami S, Segall JE, Lauffenburger DA, Bresnick AR, Gertler FB, Condeelis JS (2011) Mena invasive (MenaINV) promotes multicellular streaming motility and transendothelial migration in a mouse model of breast cancer. *J Cell Sci* 124(Pt 13):2120–2131
 13. Agarwal S, Gertler FB, Balsamo M, Condeelis JS, Camp RL, Xue X, Lin J, Rohan TE, Rimm DL (2012) Quantitative assessment of invasive mena isoforms (Menacalc) as an independent prognostic marker in breast cancer. *Breast Cancer Res* 14(5):R124
 14. Forse CL, Agarwal S, Pinnaduwege D, Gertler F, Condeelis JS, Lin J, Xue X, Johung K, Mulligan AM, Rohan TE, Bull SB, Andrulis IL (2015) Menacalc, a quantitative method of metastasis assessment, as a prognostic marker for axillary node-negative breast cancer. *BMC Cancer* 15:483
 15. Philippar U, Roussos ET, Oser M, Yamaguchi H, Kim H-D, Giampieri S, Wang Y, Goswami S, Wyckoff JB, Lauffenburger DA, Sahai E, Condeelis JS, Gertler FB (2008) A mena invasion isoform potentiates EGF-induced carcinoma cell invasion and metastasis. *Dev Cell* 15(6):813–828
 16. Pignatelli J, Goswami S, Jones JG, Rohan TE, Pieri E, Chen X, Adler E, Cox D, Maleki S, Bresnick A, Gertler FB, Condeelis JS, Oktay MH (2014) Invasive breast carcinoma cells from patients exhibit MenaINV- and macrophage-dependent transendothelial migration. *Sci Signal* 7(353):ra112
 17. Roussos ET, Goswami S, Balsamo M, Wang Y, Stobezki R, Adler E, Robinson BD, Jones JG, Gertler FB, Condeelis JS, Oktay MH (2011) Mena invasive (Mena(INV)) and Mena11a isoforms play distinct roles in breast cancer cell cohesion and association with TMEM. *Clin Exp Metastasis* 28(6):515–527
 18. Gertler FB, Niebuhr K, Reinhard M, Wehland J, Soriano P (1996) Mena, a relative of VASP and Drosophila Enabled, is implicated in the control of microfilament dynamics. *Cell* 87(2):227–239
 19. Lebrand C, Dent EW, Strasser GA, Lanier LM, Krause M, Svitkina TM, Borisy GG, Gertler FB (2004) Critical role of Ena/VASP proteins for filopodia formation in neurons and in function downstream of netrin-1. *Neuron* 42:37–49
 20. Bear JE, Loureiro JJJ, Libova II, Fässler RR, Wehland JJ, Gertler FB (2000) Negative regulation of fibroblast motility by Ena/VASP proteins. *Cell* 101(7):717–728
 21. Goswami S, Philippar U, Sun D, Patsialou A, Avraham J, Wang W, Di Modugno F, Nistico P, Gertler FB, Condeelis JS (2009) Identification of invasion specific splice variants of the cytoskeletal protein Mena present in mammary tumor cells during invasion in vivo. *Clin Exp Metastasis* 26(2):153–159
 22. Lin EY, Jones JG, Li P, Zhu L, Whitney KD, Muller WJ, Pollard JW (2003) Progression to malignancy in the polyoma middle T oncoprotein mouse breast cancer model provides a reliable model for human diseases. *Am J Pathol* 163(5):2113–2126
 23. Valastyan S, Weinberg RA (2011) Tumor metastasis: molecular insights and evolving paradigms. *Cell* 147:275–292
 24. Chaffer CL, Marjanovic ND, Lee T, Bell G, Kleer CG, Reinhardt F, D'Alessio AC, Young RA, Weinberg RA (2013) Poised chromatin at the ZEB1 promoter enables breast cancer cell plasticity and enhances tumorigenicity. *Cell* 154(1):61–74
 25. Brugnoli F, Grassilli S, Piazzini M, Palomba M, Nika E, Bavelloni A, Capitani S, Bertagnolo V (2013) In triple negative breast tumor cells, PLC-β2 promotes the conversion of CD133high to CD133low phenotype and reduces the CD133-related invasiveness. *Mol Cancer* 12:165
 26. Chen Y-C, Chen Y-W, Hsu H-S, Tseng L-M, Huang P-I, Lu K-H, Chen D-T, Tai L-K, Yung M-C, Chang S-C, Ku H-H, Chiou S-H, Lo W-L (2009) Aldehyde dehydrogenase 1 is a putative marker for cancer stem cells in head and neck squamous cancer. *Biochem Biophys Res Commun* 385(3):307–313
 27. Ginestier C, Hur MH, Charafe-Jauffret E, Monville F, Dutcher J, Brown M, Jacquemier J, Viens P, Kleer CG, Liu S, Schott A, Hayes D, Birnbaum D, Wicha MS, Dontu G (2007) ALDH1 is a marker of normal and malignant human mammary stem cells and a predictor of poor clinical outcome. *Cell Stem Cell* 1(5):555–567
 28. Murphy PA, Kim TN, Lu G, Bollen AW, Schaffer CB, Wang RA (2012) Notch4 normalization reduces blood vessel size in arteriovenous malformations. *Sci Transl Med* 4(117):117ra8
 29. Roussos ET, Goswami S, Balsamo M, Wang Y, Stobezki R, Adler E, Robinson BD, Jones JG, Gertler FB, Condeelis JS, Oktay MH (2011) Mena invasive (Mena(INV)) and Mena11a isoforms play distinct roles in breast cancer cell cohesion and association with TMEM. *Clin Exp Metastasis* 28(6):515–527
 30. Shapiro IM, Cheng AW, Flytzanis NC, Balsamo M, Condeelis JS, Oktay MH, Burge CB, Gertler FB (2011) An EMT-driven alternative splicing program occurs in human breast cancer and modulates cellular phenotype. *PLoS Genet* 7(8):e1002218
 31. Di Modugno F, Iapicca P, Boudreau A, Mottolese M, Terrenato I, Perracchio L, Carstens RP, Santoni A, Bissell MJ, Nisticò P (2012) Splicing program of human MENA produces a previously undescribed isoform associated with invasive, mesenchymal-like breast tumors. *Proc Natl Acad Sci USA* 109(47):19280–19285
 32. Zardavas D, Baselga J, Piccart M (2013) Emerging targeted agents in metastatic breast cancer. *Nat Rev Clin Oncol* 10(4):191–210